Desalination and Water Treatment
www.deswater.com
doi: 10.5004/dwt.2020.25995

198 (2020) 335–344
September

Adsorption isotherm, kinetic modeling, and mechanism of neutral red on *Auricularia auricularia*

Yingjie Dai[a], Jingjing Li[a], Qiya Sun[b], Zhihua Liu[a,*]

[a]*College of Resources and Environment, Northeast Agricultural University, No. 600 Changjiang Road, Xiangfang District, Harbin 150030, China, Tel./Fax: +86 451 5519 0825; emails: zhihua-liu@neau.edu.cn (Z. Liu), dai5188@hotmail.com (Y. Dai), 67384708@qq.com (J. Li)*
[b]*College of Environmental Science and Engineering, Tongji University, No. 1239 Siping Road, Yangpu District, Shanghai 200082, China, email: 2274657233@qq.com (Q. Sun)*

Received 6 September 2019; Accepted 18 April 2020

ABSTRACT

In this study, two kinds of *Auricularia auricularia* (*A. auricularia*) were selected as biosorbents, and their adsorption behavior to neutral red in aqueous solution was analyzed. The maximum adsorption capacity of AA-1 and AA-Se for neutral red can reach 196.08 and 222.22 mg/g, respectively. Characterized the physicochemical properties of AA-1 and AA-Se by elemental analysis, Fourier transform infrared and scanning electron microscopy. Batch tests have shown that the pH of the solution can greatly affect the adsorption effect. The adsorption process conforms to the pseudo-second-order kinetic model and the Langmuir adsorption isotherm model. This study aims to explore a new efficient and cost-effective adsorbent that not only has high adsorption capacity but also consumes less energy, and has broad application prospects in the treatment of water pollutants.

Keywords: Adsorbent; Application; Dye; Isotherm model; Kinetics

1. Introduction

Auricularia auricularia (*A. auricularia*) is one of the representative fungi of basidiomycotina, mainly composed of mycelium and fruiting body [1]. It is one of the four most important cultivated edible fungi in the world [2]. AA grows on the rot, it looks like human ear, so the name is fungus. Fresh *A. auricularia* is a gelatinous sheet, translucent, elastic, smooth, and concave on the ventral surface, slightly curled on the edges, raised on the back, and very finely fluffy, dark brown, or brown. It shrinks to a horny shape after drying, is hard and brittle, has a good taste, and is good for health [3]. The origin of *A. auricularia* is mainly in China, Thailand, Japan, and other countries in Asia. Among them, China has the highest *A. auricularia* production and the quality is far ahead. Among them, Heilongjiang, Hubei, Yunnan, and other provinces have a lot of *A. auricularia* production and good quality, which is famous at home and abroad [4]. *A. auricularia* is a nutrient-rich and pharmacological edible fungus. A large number of studies have shown that *A. auricularia* has anti-coagulation, anti-tumor, improve human immunity, anti-oxidation and anti-aging, lower blood cholesterol, antibacterial effects, and other functional activities [2]. Furthermore, the rubber contained in *A. auricularia* can absorb and dissolve the dust and impurities absorbed by the human body, and has good health care functions for workers with large dust and poor working environment [5]. It can be used as biomass adsorbent. Song et al. [6] used NaOH-modified *A. auricularia* matrix waste to adsorb cadmium(II) in water. The results demonstrated that its adsorption amount was 35.51 mg/g, and the adsorption amount was still 14.02 mg/g after three repeated uses.

* Corresponding author.

Previous report have shown that the adsorption of Cr(VI) by *A. auricularia* modified with cationic surfactant has a good effect [7].

In recent years, the use of synthetic chemical dyes in industrial processes such as textile, printing, and pulp manufacturing has increased significantly [8]. It is estimated that more than 7×10^5 tons of approximately 10^5 commercial dyes are produced each year [9]. With the development of industry and technology, the problem of water pollution containing dyes has attracted more and more attention [10]. Most dyes are very toxic substances that can cause permanent health damage to the eyes and skin of humans and animals [11]. Due to its high chemical and photolysis stability, it has extended and complex degradation processes, forming potential carcinogenic compounds that may eventually enter the food chain, threatening both human beings health and the environment [8]. In addition, the presence of dyes in water leads to increased turbidity, blocking the penetration of sunlight and oxygen, resulting in reduced photosynthesis in aquatic ecosystems [9]. Therefore, removing them from industrial wastewater is a major environmental problem [8].

Neutral red (NR) is a kind of water-soluble cationic dye. It is a pH indicator that changes from red to yellow in the pH range of 6.8–8.0 [12]. The structure of NR is shown in Fig. 1. The toxicity of dyes can be explained by the fact that carbon monoxide (CO), carbon dioxide (CO_2), nitrogen oxides, and hydrogen chloride are released during decomposition [13]. Therefore, the adsorption of NR dyes has achieved attention from all over the world.

Recently, there is an increasing demand for 10 effective and economical technologies for removing water-based environmental dyes in the world. Various technologies, including adsorption, flocculation, photodegradation, ozonation, and anaerobic treatment, utilized to study the adsorption of dyes from aqueous solutions [14]. Compared with the others methods, adsorption is the well-known and economical techniques for dye removal due to its simple, efficient, economical, and environmentally friendly properties [15,16]. Activated carbon is considered by researchers to be the most efficient adsorbent in organic adsorbents because of their good adsorption capacity for organic targets [17]. However, activated carbon is limited by its high cost [18]. Therefore, there is a need to find new, readily available, and highly efficient adsorbents. From an environmental point of view, due to low cost, wide source, and simple production process, biomass materials, or modified biomass materials have been increasingly used in the treatment of printing and dyeing wastewater [19]. At present, the biomass materials used for adsorption mainly include coconut leaf [20], rice husk [21], corn stalk [22], bagasse [23], walnut shell [16], and banana peel [17]. However, there have been few reports on the use of fungi to adsorb dyes.

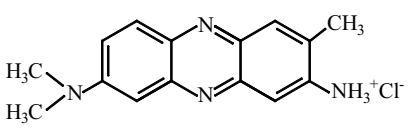

Fig. 1. Structural formula of NR.

In this paper, two kinds of *A. auricularia* (AA-1 and AA-Se) are used as adsorbents to experimentally remove the NR from water. The prepared adsorbents were characterized using various analytical techniques and the different pH on this study was carried out. Kinetic data and isotherm parameters were applied to understand the adsorption mechanism for NR. The results illustrated that *A. auricularia* is an effective adsorbent in water environment, which is of great significance for the further application of *A. auricularia* in dye removal.

2. Materials and methods

2.1. Reagents

The purity of all chemicals in this study were higher than 99.0%. NR was got from Fuchen Chemical Co., (Tianjin, China). The NR was dissolved into 1,000 mg/L with deionized water, the NR concentration required for the experiment was obtained by diluting the stock solution with distilled water. The adjustment of solution pH was utilized HCl and NaOH.

2.2. Preparation of adsorbents

A. auricularia were obtained from the Baoqing Cooperative of Harbin, China. After washed, the *A. auricularia* were dried at 103°C for 48 h, then pulverized for storage.

2.3. Characterization of AA-1 and AA-Se

The contents data of mineral elements of samples were obtained by inductively coupled plasma-atomic emission spectroscopy (ICP-AES, Vista-MPX, USA). The morphology of AA-1 and AA-Se were observed by scanning electron microscopy (SEM, ZEISS EVO 60, Germany). The surface functional groups of the samples were identified by Fourier transform infrared spectroscopy (FTIR, Nicolet 6700, USA). The distribution of the zeta potential and the particle size distribution of the AA-1 and AA-Se was measured using a Delsa™ nanoZeta potential and a submicron particle size analyzer. The common elements such as C, N, and H of samples were determined by an elemental analyzer (PerkinElmer 2400 Series II, MA, USA).

The surface zero charge point (pH_{pzc}) of AA-1 and AA-Se was determined by the pH drift method. Configure 0.1 mol/L NaCl solution, their pH values were adjusted to 2.0, 4.0, 6.0, 8.0, 10.0, and 12.0 by NaOH or HCl (0.1–1.0 mol/L) solution, respectively. Add 100 mg of AA-1 and AA-Se to several flasks, and add 50 mL of NaCl (0.1 mol/L) solution with different initial pH (pH_i). Then, the Erlenmeyer flask was placed at 25°C and 165 rpm for shaking reaction. The pH value (pH_f) after 48 h of the NaCl solution was determined. Taking pH_i as the abscissa and $\Delta pH = pH_i - pH_f$ as the ordinate, the pH at $pH_i - pH_f = 0$ (See Fig. 2) is the pH_{pzc} of the adsorbent.

2.4. Batch experiments

Samples were weighted using the coning and quartering method for an inhomogeneous adsorbent material.

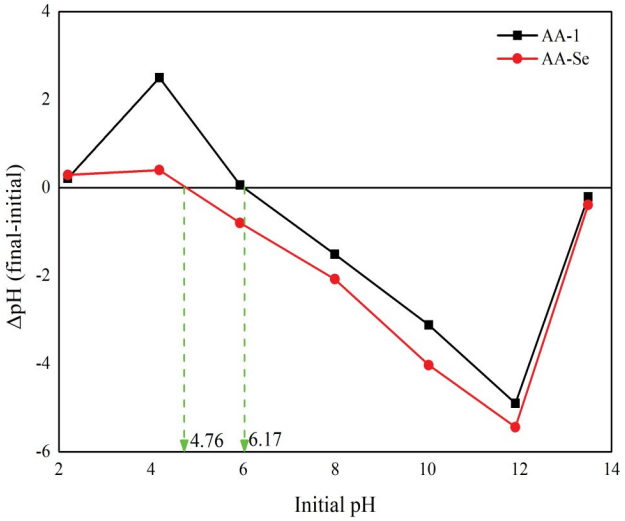

Fig. 2. pH_{pzc} of AA-1 and AA-Se.

20 mg of AA-1 and AA-Se were, respectively, added into a 100 mL flask, and 25 mL of a 5–100 mg/L NR solution was added. The solution pH was changed from 2.0 to 12.0 with 0.1 mol/L HCl or 0.1 mol/L NaOH. The adsorption was shaken at 165 rpm for 5–120 min at 25°C, filtered, and the filtrate was placed in a cuvette, and the absorbance was determined at a wavelength of 530 nm using a UV-vis spectrophotometer (V-1800, Shimadzu, Japan). The NR concentration was calculated from the NR standard operating curve. The formulas for calculating the adsorption amount (q_t, mg/g) and removal rate (R, %) of the adsorbent at time t of NR are using Eqs. (1) and (2):

$$q_e = \frac{V\left(C_0 - C_t\right)}{W} \tag{1}$$

$$R = \frac{C_0 - C_t}{C_0} \times 100\% \tag{2}$$

In the formula, C_0 and C_t are the concentrations of NR at the initial and time t, respectively, mg/L; t is the adsorption time, min; V is the volume of solution, L; and W is the adsorbent addition amount, g.

2.5. Adsorption kinetics models

Adsorption kinetics can well-describe the performance and adsorption mechanism of adsorbents [24,25]. In this paper, five kinetic models: the pseudo-first-order, pseudo-second-order, Elovich, intra-particle diffusion, and liquid film diffusion, were used to describe the kinetics of NR adsorption by two species of *A. auricularia* [26]. The formulas of each model are shown in Eqs. (3)–(7), respectively.

Pseudo-first-order:

$$Q_t = Q_e\left(1 - \exp\left(-k_1 t\right)\right) \tag{3}$$

Pseudo-second-order:

$$Q_t = \frac{k_2 Q_e^2 t}{1 + k_2 Q_e t} \tag{4}$$

Elovich equation:

$$Q_t = \frac{1}{b}\ln ab + \frac{1}{b}\ln t,\ t_0 = \frac{1}{ab} \tag{5}$$

Intra-particle diffusion:

$$Q_t = k_i t^{0.5} + c \tag{6}$$

Liquid film diffusion:

$$\ln(1 - F) = -k_{fd} t,\ F = \frac{Q_t}{Q_e} \tag{7}$$

where Q_e and Q_t (mg/g) means the adsorption capacity at equilibrium time and time t (min); k_1 (min^{-1}) and k_2 (g mg^{-1} min^{-1}) are the adsorption rate constant of the two kinetic models, respectively; a is the rate constant of chemisorption and b is the constant of the surface coverage; k_i (mg g^{-1} $min^{0.5}$) is the intra-particle diffusion rate constant, c (mg/g) is a constant related to the boundary layer thickness; where k_{fd} is adsorption rate constant, F is the fractional achievement of equilibrium at time t.

The R^2 is used to describe the kinetic model fitting effect [26,27]. The R^2 is shown in Eq. (8):

$$R^2 = 1 - \frac{\sum\left(y - \hat{y}\right)^2}{\sum\left(y - \bar{y}\right)^2} \tag{8}$$

where y is the observed value, $\hat{y}$ is the fitted value, and $\bar{y}$ is the mean of observed values.

2.6. Adsorption isotherm models

The Langmuir, Freundlich, and Temkin isotherm models were used to study the adsorption behavior of *A. auricularia* on NR, the formulas of which are shown as follows [22,27].

The Langmuir equation is shown as Eq. (9):

$$Q_e = \frac{Q_m K_L C_e}{1 + K_L C_e} \tag{9}$$

where Q_m is the theoretical maximum adsorption amount, mg/g; K_L is the Langmuir model constant, the unit is determined according to the specific conditions; C_e is the NR mass concentration at the equilibrium of adsorption, mg/L.

The Freundlich equation is shown as Eq. (10):

$$Q_e = K_F C_e^{\frac{1}{n}} \tag{10}$$

where K_F is a Freundlich constant related to the adsorption capacity; n is a constant about the adsorption strength of the adsorbent.

The Temkin isotherm model equation is shown as Eq. (11):

$$Q_e = \frac{RT}{b_T}\ln\left(K_T C_e\right) \tag{11}$$

where R is the universal gas constant (8.314 J/mol K), T is the temperature in terms of Kelvin, b_T is Temkin constant, K_T is equilibrium bond constant related to the maximum energy of bond.

3. Results and discussion

3.1. Characterizations of AA-1 and AA-Se

The content of Se was 0.98 mg/kg, which was significantly higher than that of AA-1 (0.04 mg/kg). As one of the essential micronutrients for humans and animals, Se is involved in the synthesis of more than 30 proteins and enzymes in mammals. It has various biological functions such as anti-mutation, anti-oxidation, promotes *in vivo* inactivation of carcinogens, anti-cell proliferation, and enhances immunity, etc [28]. Studies have shown that the main Se-containing component of AA-Se is organic, in which the content of protein selenium is the highest, and the distribution of Se is also found in non-protein or polysaccharide [29]. Some scholars believe that organic Se can form a Se-heavy metal complex with heavy metals Hg, Cd, etc. to reduce the bioavailability of heavy metals [28]. The emergence of AA-Se provides a new and easy way to resist heavy metals.

Figs. 3a and b show the SEM images of AA-1 and AA-Se, respectively. The SEM images of the two materials showed that the surface of the adsorbent is rough, uneven, and has a mountain-like shape, and the surface contains pore structure, and the pore size distribution is uneven, which may provide more adsorption sites for adsorbing NR. The FTIR of AA-1 and AA-Se before and after adsorbing NR are shown in Figs. 4a and b, respectively. As can be seen from the figures, the FTIR of AA-1 differs from that of AA-Se. Both AA-1 and AA-Se have typical functional group peaks. The shift of the main peak and the specific functional group corresponding to FTIR are shown in Table 1. The main functional groups of AA-1 include 3,460.86 cm^{-1} (–OH functional group), 2,297.15 and 2,853.36 cm^{-1} (lipid CH functional group), 1,655.06 cm^{-1} (C=O stretching or aromatic C=C and C=O/C=C expansion and contraction), 1,458.52 cm^{-1} (CH alkane on the aromatic ring), 1,378.02 cm^{-1} (CH bending, symmetric bending of $–CH_3$), 1,244.06 cm^{-1} ($–SO_3$ expansion/P=O), 1,165.31 cm^{-1} (COC of polysaccharide), 1,060.72 cm^{-1} (COH stretching), 616.57 cm^{-1} (–CC–) [30].

After AA-1 adsorbed NR, there was no change in the type of functional group, and only the position of the absorption peak of some functional groups changed. Fig. 4 shows that the functional groups of AA-Se mainly include 3,418.81 cm^{-1} (–OH functional group), 2,926.18 cm^{-1} (lipid CH functional group), 1,735.78 cm^{-1} (–COH), and 1,655.06 cm^{-1} (C=O stretching or aromatic C=C and C=O/C=C stretching), 1,560.44 cm^{-1} (secondary amine group), 1,377.69 cm^{-1} (CH bending, symmetric bending of $–CH_3$), 1,254.48 cm^{-1} (CN stretching)), 1,064.40 cm^{-1} (COH stretching), 605.45 cm^{-1} (Fe–O) [30,31]. After adsorption of NR, the functional group of AA-Se shifts or disappears, for example, 3,415.81 → 3,424.75; 1,735.78 → 1,739.94; 1,655.06 cm^{-1} → 1,636.83; 1,254.48 → 1,250.33; 605.45 → 599.09 cm^{-1}, and the peak of 1,560.44 cm^{-1} disappeared. Thus, the –OH/NH, –COH, C=C, –CO, and benzene ring skeletons in AA-Se participate in the reaction with NR.

3.2. Effect of pH

With different initial pH of dyes solution, the adsorption behaviors have different feature [11]. Not only the dissociation and functional groups on the surface of adsorbents at their active sites is affected by the pH of solution, but also the ionization and structural changes of dye molecules [32]. The pH_{pzc} is a significance feature that could determined the surface charge of adsorbents [33]. As shown in Fig. 2, the pH_{pzc} of AA-1 and AA-Se are 6.17 and 4.76, respectively.

The results are shown in Fig. 5. Under acidic conditions, the adsorption ratio is low, with the increases of solution pH, the adsorption ratio increases. When the pH value is higher than 6.0, there is little effect on the adsorption rate of NR adsorbed by AA-1 and AA-Se of the changed pH, and the removal ratio of NR to AA-1 and AA-Se reaches 92.30% and 90.10% at pH 6.0 and 10.0, respectively. As the pH gradually increases, the removal ratio of NR even tends to decrease slowly.

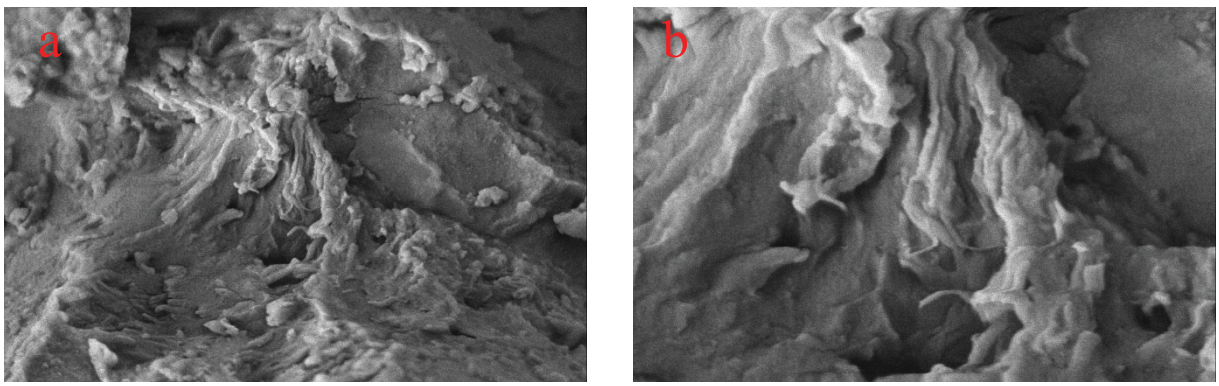

Fig. 3. Scanning electron microscopy images of AA-1 (a) and AA-Se (b).

Table 1
Changes of main functional groups before and after adsorption

Wavenumber (cm^{-1})	AA-1 (cm^{-1})	AA-1+NR (cm^{-1})	AA-Se (cm^{-1})	AA-Se+NR (cm^{-1})	Assignment
3,750–3,000	3,460.86	3,422.54	3,415.81	3,424.75	–OH/N–H
3,000–2,700	2,927.15	2,925.04	2,926.18	2,926.84	$–CH_3$
	2,853.36	2,854.19			C–H stretching
1,900–1,650	1,743.85	1,743.02	1,735.78	1,739.94	–COH
1,680–1,620	1,655.06	1,655.00	1,655.06	1,636.83	C=O
1,620–1,450			1,560.44		Benzene ring skeleton
	1,458.52	1,458.62			
1,375	1,378.02	1,375.94	1,377.69	1,378.26	C–H deformation
1,275–1,210	1,244.06	1,274.01	1,254.48	1,250.33	Asymmetric stretching vibration of –COC–
1,162	1,165.31	1,165.31			–CO stretching
1,050	1,060.72	1,064.90	1,036.40	1,036.39	Si–O–Si/C–O
1,000–650	869.92	869.92			Benzene ring substitution
	804.54	800.45			
	616.57	608.40	605.45	599.09	

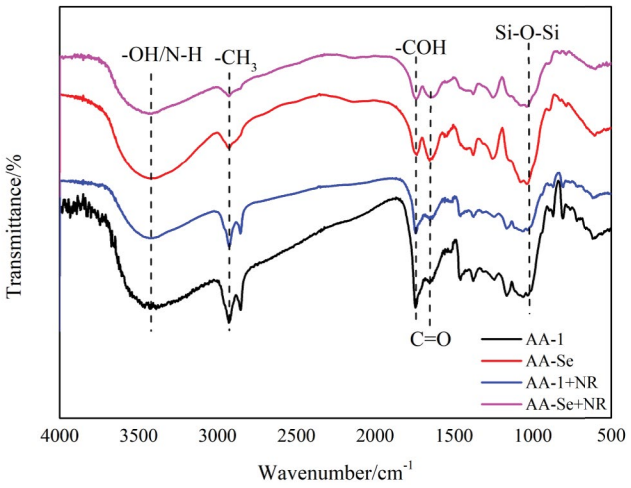

Fig. 4. FTIR spectra of AA-1 and AA-Se.

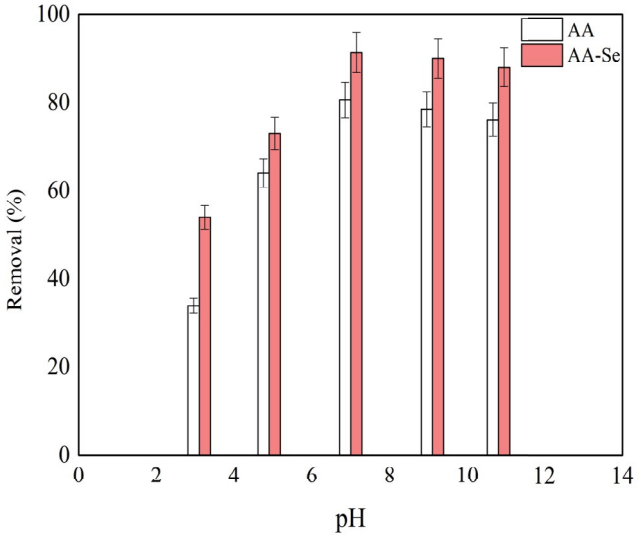

Fig. 5. Effect of pH on the adsorption of NR by AA-1 and AA-Se.

Based on the pH_{pzc} of the biosorbent could explain this phenomenon [34]. With the increases of pH, due to the increased negative charge, more cationic dyes are attached on the adsorbent surface [22]. At pH < pH_{pzc}, on the one hand, the sample presents the positively charged, and the neutral red surface of the cationic dye is also positively charged, and the electrostatic repulsion inhibits the smooth progress of adsorption. On the other hand, the H^+ concentration is high, competing with the positively charged NR cation of the vacancy adsorption site, and at the same time hinders the dissociation of the reactive functional group, leading to the low adsorption capacity [35]. The higher pH, the lower concentration of H^+ when pH > pH_{pzc}, and negative enhancement of the surface of the adsorbent, which is beneficial for the adsorption of NR onto AA-1 and AA-Se. Therefore, the adsorption rate increases due to an increase in electrostatic attraction [36].

In addition, it can be found from experiments that *A. auricularia* contains active sites capable of binding NR, and the removal rate and adsorption amount of NR are related to the chemical environment of the solution and the number of active sites. From the characterization analysis of AA-1 and AA-Se, AA-1, and AA-Se contains a large amount of polysaccharides and various amino acids, and contains amino, aldehyde, ketone, or carboxylic acid groups, such as –NH, $RC–NH_2$, –OH, C=O, and COOH, which are important groups for adsorption dyes. These functional groups are often negatively charged in aqueous solution, while NR dissociates in aqueous solution and exists in the form of a cation. Therefore, under acidic conditions, the AA-1 and AA-Se surface is surrounded by more protons, competing with NR, and binding to the active sites on the surface of the biosorbent. However, when the pH of the solution environment is high, the surface of AA-1 and AA-Se is negatively charged, and more dye cations are combined by electrostatic attraction [37].

3.3. Adsorption kinetics

The adsorption kinetics and adsorption rate-limiting steps have significance meanings for understand the mechanisms of adsorption. The dynamic adsorption processes of NR onto AA-1 and AA-Se are shown in Fig. 6a. The curves revealed similar trends that the adsorption ratio increased quickly at the early stage while it gradually stable since the decreased accessible adsorption sites and this phenomenon often achieved in previous reports [38].

The pseudo-first-order, pseudo-second-order, and Elovich kinetics models were utilized for the further understand of the adsorption behavior. The results are shown in Figs. 6b, c, and f, the parameters are shown in Table 2.

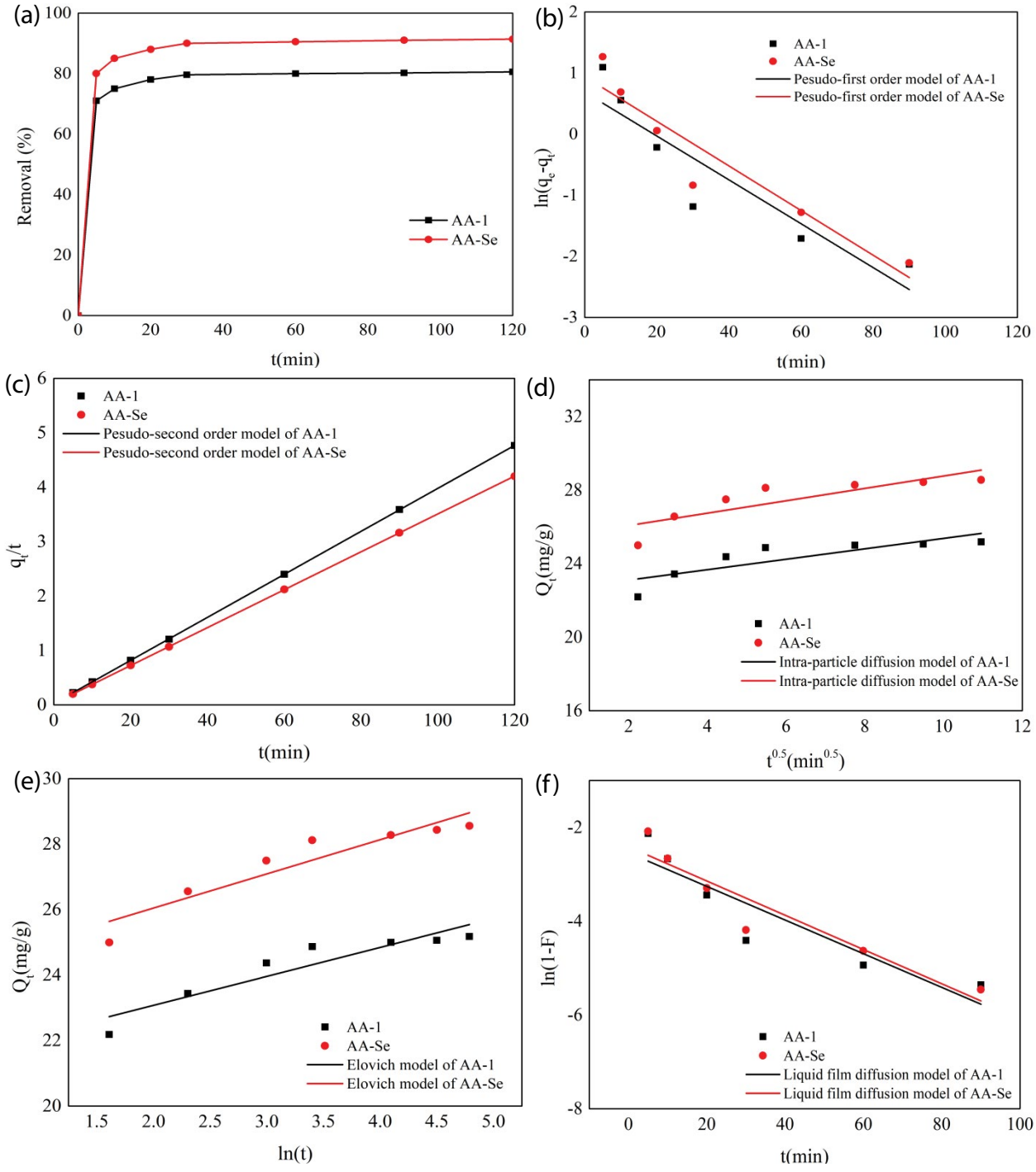

Fig. 6. Effect of adsorption time on NR removals in the range of 0–120 min plots for the adsorption of NR on AA-1 and AA-Se (a) effect of adsorption time, (b) pseudo-first-order, (c) pseudo-second-order, (d) intra-particle diffusion, (e) liquid film diffusion, and (f) Elovich.

Table 2
Kinetics related parameters of AA adsorption NR

Models and parameters	AA-1	AA-Se
Q_e (Experimental value)	25.18	28.56
Pseudo-first-order		
Q_e (mg/g)	1.9909	2.5656
k_1 (1/min)	0.0359	0.0365
R^2	0.8439	0.8983
Pseudo-second-order		
Q_e (mg/g)	25.3164	28.7356
k_2 (g/mg min)	0.0547	0.0434
R^2	1.0000	1.0000
Elovich		
a	2.53×10^{10}	9.72×109
b	1.1299	0.9579
R^2	0.8049	0.8729
Intra-particle diffusion		
c (mg/g)	22.5382	25.4009
k_i (mg·g^{-1}·min$^{0.5}$)	0.2837	0.3369
R^2	0.6396	0.6628
Liquid film diffusion		
k_{fd}	0.0359	0.0365
R^2	0.8049	0.8729

Clearly, this experiment data were well-matched to the pseudo-second-order due to the R^2 of pseudo-second-order was higher than that of the others isotherm model and the Q_e was similar with the experiment value. This results could demonstrated that the adsorption processes of NR onto AA-1 and AA-Se were chemical processes [26].

The rate-limiting of the adsorption typically divided into four steps: first, bulk transport; second, film transport; third, intra-particle transport; last, adsorption on the adsorbent. The film transport and intra-particle transport models were carried out in this study to understand the rate-limiting step and the adsorption mechanisms. The results are shown in Figs. 6d and e, and the parameters of models are shown in Table 2. The film transport was the rate-limiting step due to the R^2 of film transport was higher than that of intra-particle and the plots of intra-particle were not passed the origin.

3.4. Adsorption isotherm

Langmuir, Freundlich, and Temkin isotherm models were carried out in this study. Langmuir isotherm model presumes that the process is the monolayered adsorbents on the homogeneous surface [39]. Freundlich isotherm model presumes that it occurs with a heterogeneous surface [40]. Temkin model could prove the interplay between the samples and contaminants, and the D–R isotherm is applied to analysis whether the adsorption is physically or chemically [41]. In this study, the results are shown in Fig. 7 and the parameters are shown in Table 3. The results illustrated that the experiment data was well-fitted to the three isotherm models at the same time due to the R^2 were higher than 0.95. The K_L of Langmuir model were higher than 0 could claimed that the adsorption were favorable in this study [42]. According to the Q_m calculated by the equation of Langmuir model, the maximum adsorption capacity of AA-1 and AA-Se were 196.08 and 222.22 mg/g, respectively. The $1/n$ value of Freundlich demonstrated that heterogeneity factor presents high heterogeneity studies [43]. It could be explained by that the adsorption processes of NR onto AA-1 and AA-Se were controlled by multiple adsorption mechanisms.

3.5. Adsorption mechanism

Adsorption of NR by AA-1 and AA-Se is a complex process involving multiple steps and multiple mechanisms work together. According to influencing factors, kinetics, isotherms, and instrumental characterization, the mechanism of adsorbent removal of dyes involves electrostatic interaction, ion exchange, hydrogen bonding, and π–π interaction [31]. The specific mechanism also depends on the nature of the adsorbent and the solution environment.

Solution pH is a key factor affecting NR removal. Electrostatic action is an important mechanism affecting NR removal, but it is not the only mechanism. AA-1 and AA-Se contain a large amount of polysaccharides and various amino acids, and contain many important groups such as –NH, R–C–NH$_2$, –OH, –COH, COOH. These functional groups are often negatively charged in aqueous solution, while NR dissociates in aqueous solution and exists in the form of a cation. Therefore, there is an electrostatic interaction between the adsorbent and NR. FTIR analysis showed that the functional groups in AA-1 and AA-Se played a key role in NR adsorption, including aromatic skeleton vibration, C–H, C–O, Si–O–Si changes, involving π–π stacking, hydrogen bonding, etc. The aromatic benzene rings of AA-1 and AA-Se easily form π–π stacking with the benzene ring of NR.

The kinetic results (pseudo-second-kinetics and Elovich model) show that the chemisorption mechanism plays an important role in the adsorption of NR by AA-1 and AA-Se. The mechanism involved in chemisorption is the formation of covalent bonds and ion exchange. The adsorption isotherm results show that the adsorption of NR by AA-1 and AA-Se is based on electrostatic adsorption.

In addition, studies have shown that some proteins and polysaccharides contained in the cell wall can act as a ligand to interact with the metal to immobilize the metal on the cell wall [28]. Based on this, it is speculated that NR may cooperate with proteins and polysaccharides on the cell wall of the adsorbent to immobilize NR on the cell wall.

Model fitting of the experimental data, we found that the saturated adsorption capacity of AA-Se is 222.22 mg/g higher than that of AA-1 (196.08 mg/g). This may be caused by a variety of reasons. First, the content of cysteine in AA-Se was 1.42 g/kg higher than that of AA-1 (0.94 g/kg). Cysteine is an amino acid commonly found in many organisms. It is found in many proteins, glutathione (GPH), and forms

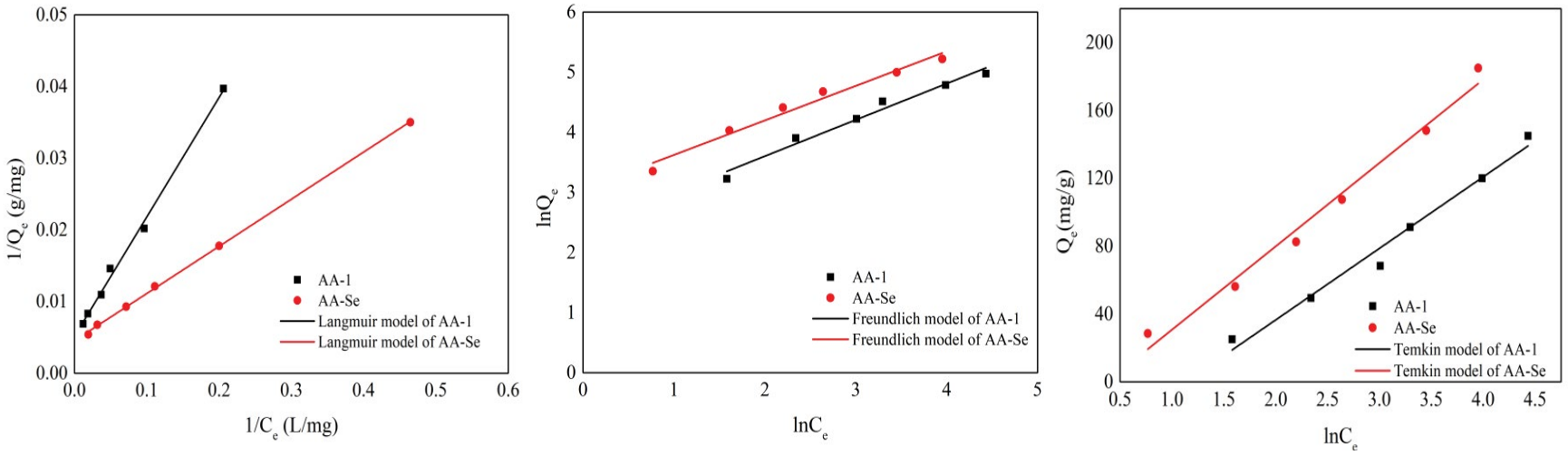

Fig. 7. Isothermal adsorption model for adsorption of NR by *A. auricularia*. (a) Langmuir model, (b) Freundlich model, and (c) Temkin model.

Table 3
Isothermal adsorption parameters of AA adsorption NR

Adsorbent	Langmuir model			Freundlich model			Temkin model		
	Q_m (mg/g)	K_L (L/mg)	R^2	K_F (L/mg)	$1/n$	R^2	K_T (L/g)	b_T (J/mol)	R^2
AA-1	196.08	0.0306	0.9962	10.98	0.6038	0.9757	0.3221	58.78	0.9761
AA-Se	222.22	0.0684	0.9996	21.11	0.5743	0.9761	0.688	50.41	0.9805

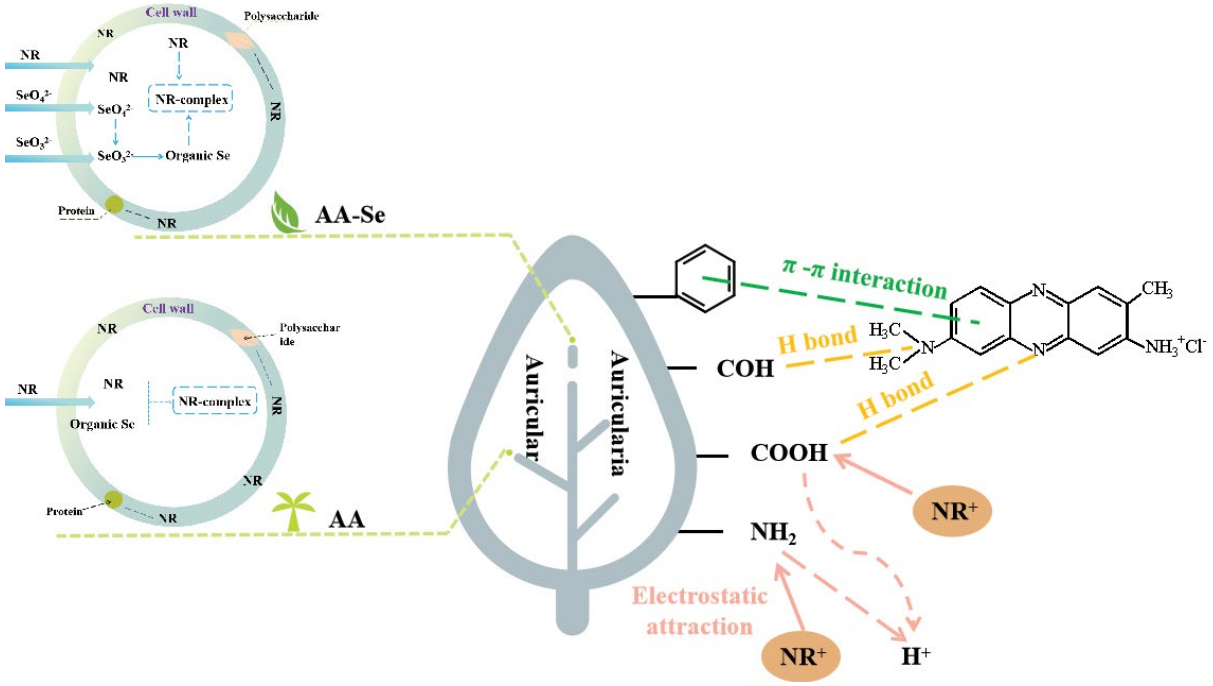

Fig. 8. Possible adsorption mechanism of NR on AA-1 and AA-Se.

insoluble thiolates with metal ions such as Ag^+, Hg^+, and Cu^{2+}. That is, R–S–M′, R–S–M″–S–R (M′, M″ are each a monovalent, divalent metal, respectively) [44]. AA-1 contains a lot of protein and GPH. Based on this, it is inferred that cysteine may react with NR^+ in the following reaction to remove NR.

Second, AA-Se contains more Se. Se is an essential component of glutathione peroxidase (GPH-Px). The main function of GPH-Px is to catalyze the reduction of GPH to form oxidized glutathione (GSSG) [45]. At the same time, the harmful peroxide is reduced to harmless hydroxyl radicals, thereby protecting the structural and functional integrity of the cell membrane [28]. The NR in the oxidation state is red, and the NR in the reduced state is colorless. Based on this, this paper speculates that the following reactions may exist.

$$\text{GSH} + \text{NR (oxidation)} \rightarrow \text{NR (reduced)} + \text{GSSG} \quad (12)$$

NR can be removed by the above oxidation–reduction reaction. Based on the experimental results, this paper speculates that there will be the above reaction, and further exploration is needed. In summary, the mechanism of AA-1 and AA-Se removal of NR includes electrostatic interaction, hydrogen bonding, and π–π stacking. The mechanism diagram is shown in Fig. 8.

4. Conclusions

This work utilized two kinds of *A. auricularia* as adsorbents to remove the NR. The maximum capacity of AA-1 and AA-Se were 196.08 and 222.22 mg/g, respectively. These two kinds of adsorbents have significance potential for the removal of contaminants due to the high adsorption capacity and the wide source. The pseudo-second kinetic model and Langmuir, Freundlich, and Temkin isotherm model were well-fitted to this experiment. The film transport was regarded as the rate-limiting step. The mechanism of this adsorption included electrostatic interaction, hydrogen bonding, and π–π stacking.

References

[1] H.B. Jiang, The Role and Mechanistic Investigation of Mixed Powder Ginseng and Auricularia on Hypolipidemic Activity, Ph. D. Dissertation, Jilin University, 2016.
[2] Y.L. Zhang, Y. Mu, Y.J. Li, P. Wan, L. Feng, H. Lei, Effects of geographical environment and genotype on nutritional contents, texture and microstructure of *Auricularia auricula*-judae, Food Sci., 39 (2018) 233–239.
[3] Available at: http://www.baike.com/wiki/%E9%BB%91%E6%9C%A8%E8%80%B3
[4] Y.J. Liu, Study on Chemical Components and Pharmacological Activities of *Auricularia auricula*, Ph. D. Dissertation, Shandong Institute of Light Industry, 2011.
[5] Q. Zheng, Z.G. Wu, Advances in research and application of *Auricularia auricula* in recent years, Light. Ind. Sci. Technol., 11 (2017) 11–14.
[6] T. Song, J.S. Liang, X. Bai, Y. Li, Y.N. Wei, S.Q. Huang, L.Y. Dong, J.J. Qu, Y. Jin, Biosorption of cadmium ions from aqueous solution by modified *Auricularia auricular* matrix waste, J. Mol. Liq., 241 (2017) 1023–1031.
[7] Y. Li, Y.N. Wei, S.Q. Huang, X.S. Liu, Z.H. Jin, M. Zhang, J.J. Qu, Y. Jin, Biosorption of Cr(VI) onto *Auricularia auricula* dreg biochar modified by cationic surfactant: characteristics and mechanism, J. Mol. Liq., 269 (2018) 824–832.
[8] M.A. Rauf, I.A. Shehadi, W.W. Hassan, Studies on the removal of neutral red on sand from aqueous solution and its kinetic behaviour, Dyes Pigm., 75 (2007) 723–726.
[9] P.C. Bhomick, A. Supong, M. Baruah, C. Pongener, Pine cone biomass as an efficient precursor for the synthesis of activated biocarbon for adsorption of anionic dye from aqueous solution: isotherm, kinetic, thermodynamic and regeneration studies, Sustainable Chem. Pharm., 10 (2018) 41–49.

[10] W.Q. Wang, C.C. Li, J.L. Yao, B. Zhang, Y.T. Zhang, J.D. Liu, Rapid adsorption of neutral red from aqueous solutions by $Zn_3[Co(CN)_6]_2{\cdot}nH_2O$ nanospheres, J. Mol. Liq., 184 (2013) 10–16.
[11] U.J. Etim, S.A. Umoren, U. Eduok, Coconut coir dust as a low cost adsorbent for the removal of cationic dye from aqueous solution, J. Saudi Chem. Soc., 20 (2016) 67–76.
[12] Q. Zhang, W.Q. Gong, C.X. Xie, D.J. Yang, X.Q. Ling, X.A. Yuan, S.H. Chen, X.F. Liu, Removal of neutral red from aqueous solution by adsorption on spent cottonseed hull substrate, J. Hazard. Mater., 185 (2011) 502–506.
[13] M. Iram, C. Guo, Y.P. Guan, A. Ishfaq, H.Z. Liu, Adsorption and magnetic removal of neutral red dye from aqueous solution using Fe_3O_4 hollow nanospheres, J. Hazard. Mater., 181 (2010) 1039–1050.
[14] F. Guzel, H. Saygili, G.A. Saygili, F. Koyuncu, C. Yilmaz, Optimal oxidation with nitric acid of biochar derived from pyrolysis of weeds and its application in removal of hazardous dye methylene blue from aqueous solution, J. Cleaner Prod., 144 (2017) 260–265.
[15] N. Liu, M.L. Zhu, H. Wang, H.Q. Ma, Adsorption characteristics of direct red 23 from aqueous solution by biochar, J. Mol. Liq., 223 (2016) 335–342.
[16] S. Zhao, T. Zhou, Biosorption of methylene blue from wastewater by an extraction residue of *Salvia miltiorrhiza* Bge, Bioresour. Technol., 219 (2016) 330–337.
[17] M.A. Ahmad, N. Ahamd, O.S. Bello, Adsorption kinetic studies for the removal of synthetic dye using durian seed activated carbon, J. Dispersion Sci. Technol., 36 (2015) 670–684.
[18] M.A. Zazycki, M. Godinho, D. Perondi, E.L. Foletto, G.C. Collazzo, G.L. Dotto, New biochar from pecan nutshells as an alternative adsorbent for removing reactive red 141 from aqueous solutions, J. Cleaner Prod., 171 (2018) 57–65.
[19] S.S. Fan, J. Tang, Y. Wang, H. Li, H. Zhang, J. Tang, Z. Wang, X.D. Li, Biochar prepared from co-pyrolysis of municipal sewage sludge and tea waste for the adsorption of methylene blue from aqueous solutions: kinetics, isotherm, thermodynamic and mechanism, J. Mol. Liq., 220 (2016) 432–441.
[20] A.H. Jawad, R. Abd, R.M.A. Mahmuod, M.A.M. Ishak, N.N. Kasim, K. Ismail, Adsorption of methylene blue onto coconut (*Cocos nucifera*) leaf: optimization, isotherm and kinetic studies, Desal. Water Treat., 57 (2016) 8839–8853.
[21] S.D. Ashrafi, H. Kamani, H.S. Arezomand, N. Yousefi, A.H. Mahvi, Optimization and modeling of process variables for adsorption of basic blue 41 on NaOH-modified rice huskusing response surface methodology, Desal. Water Treat., 57 (2016) 14051–14059.
[22] M.R. Fathi, A. Asfaram, A. Farhangi, Removal of direct red 23 from aqueous solution using corn stalks: isotherms, kinetics and thermodynamic studies, Spectrochim. Acta. Part A, 135 (2015) 364–372.
[23] N. Rattanachueskul, A. Saning, S. Kaowphong, N. Chumha, L. Chuemcho, Magnetic carbon composites with a hierarchical structure for adsorption of tetracycline, prepared from sugarcane bagasse via hydrothermal carbonization coupled with simple heat treatment process, Bioresour. Technol., 266 (2017) 164–172.
[24] H. Gupta, B. Gupta, Adsorption of polycyclic aromatic hydrocarbons on banana peel activated carbon, Desal. Water Treat., 57 (2016) 9498–9509.
[25] P. Zhang, Y.C. Li, H.B. Hu, J.G. Zhao, J.S. Wang, Methylene blue adsorption characteristics onto biochar derived from *Ginkgo biloba*, Environ. Pollut. Control, 11 (2017) 1229–1234.
[26] Y.Y. Zhou, X.C. Liu, Y.J. Xiang, P. Wang, J.C. Zhang, F.F. Zhang, J.H. Wei, L. Luo, M. Lei, L. Tang, Modification of biochar derived from sawdust and its application in removal of tetracycline and copper from aqueous solution: adsorption mechanism and modelling, Bioresour. Technol., 245 (2017) 266–273.
[27] K. Jung, B. Choi, M. Hwang, T. Jeong, K. Ahn, Fabrication of granular activated carbons derived from spent coffee grounds by entrapment in calcium alginate beads for adsorption of acid orange 7 and methylene blue, Bioresour. Technol., 219 (2016) 185–195.
[28] Y.N. Wan, Y. Yu, T.T. Qi, J.Y. Linghu, H.F. Li, Progress on influence mechanism of selenium on cadmium uptake and translocation in plants, Curr. Biotechnol., 7 (2017) 473–479.
[29] Y. Wu, Preliminary study on the distribution and occurrence of selenium in selenium-enriched *Auricularia auricularia*, Edible Fungi, 5 (2008) 5–6.
[30] S. Yao, M.S. Zhang, L.X. Li, Y.K. Liao, N. Zhou, S.S. Fan, J. Tang, Preparation of tea waste-nano Fe_3O_4 composite and its removal mechanism of methylene blue from aqueous solution, Environ. Chem., 37 (2018) 96–107.
[31] Y.K. Liao, L.X. Li, S.S. Fan, Removal behavior and mechanism of methylene blue in aqueous solution by rice straw and rice straw-Fe_3O_4 composite, Acta Sci. Circum., 39 (2019) 359–370.
[32] Y. Shang, J.H. Zhang, X. Wang, R.D. Zhang, W. Xiao, S.S. Zhang, R.P. Han, Use of polyethyleneimine-modified wheat straw for adsorption of Congo red from solution in batch mode, Desal. Water Treat., 57 (2016) 8872–8883.
[33] A.E. Pirbazari, E. Saberikhah, N.G.A. Gorabi, Fe_3O_4 nanoparticles loaded onto wheat straw: an efficient adsorbent for Basic Blue 9 adsorption from aqueous solution, Desal. Water Treat., 57 (2016) 4110–4121.
[34] E.K. Guechi, O. Hamdaoui, Biosorption of methylene blue from aqueous solution by potato (*Solanum tubersum*) peel: equilibrium modelling, kinetic, and thermodynamic studies, Desal. Water Treat., 57 (2016) 10270–10285.
[35] Y. Shi, Preparation of Biosorbent from Ephedra Waste and Its Adsorption Behavior for Pollutants in Aqueous Solution, Ph. D. Dissertation, Ningxia Medical University, 2015.
[36] N. Gupta, A.K. Kushwaha, M.C. Chattopadhyaya, Application of potato plant wastes for the removal of methylene blue and malachite green dye from aqueous solution, Arabian J. Chem., 9 (2016) 707–716.
[37] Q. Zhou, Study on the Biosorption of Cationic Dyes by Spent White Rot Fungi Cultivation Substrate, Ph. D. Dissertation, Wuhan University of Technology, 2012.
[38] L. Peng, Y. Ren, J. Gu, P. Qin, Q. Zeng, J. Shao, M. Lei, L. Chai, Iron improving bio-char derived from microalgae on removal of tetracycline from aqueous system, Environ. Sci. Pollut. Res., 21 (2014) 7631–7640.
[39] Y. Li, Z. Wang, X. Xie, J. Zhu, R. Li, T. Qin, Removal of norfloxacin from aqueous solution by clay-biochar composite prepared from potato stem and natural attapulgite, Colloids Surf., A, 514 (2017) 126–136.
[40] O. Pezoti, A.L. Cazetta, K.C. Bedin, L.S. Souza, A.C. Martins, L. Tais, NaOH-activated carbon of high surface area produced from guava seeds as a high-efficiency adsorbent for amoxicillin removal: kinetic, isotherm and thermodynamic studies, Chem. Eng. J., 288 (2015) 778–788.
[41] M. Naushad, Z.A. Alothman, M.R. Awual, S.M. Alfadul, T. Ahamad, Adsorption of rose Bengal dye from aqueous solution by amberlite Ira–938 resin: kinetics, isotherms, and thermodynamic studies, Desal. Water Treat., 57 (2019) 13527–13533.
[42] A.C. Martins, O. Pezoti, A.L. Cazetta, K.C. Bedin, D.A.S. Yamazaki, G.F.G. Bandoch, T. Asefa, J.V. Visentainer, V.C. Almeida, Removal of tetracycline by NaOH activated carbon produced from macadamia nut shells: kinetic and equilibrium studies, Chem. Eng. J., 260 (2015) 291–299.
[43] O.P. Junior, A.L. Cazetta, R.C. Gomes, E.O. Barizao, I.P. Souza, A.C. Martins, T. Asefa, V.C. Almeida, Synthesis of $ZnCl_2$-activated carbon from macadamia nut endocarp by microwave-assisted pyrolysis: optimization using RSM and methylene blue adsorption, J. Anal. Appl. Pyrolysis, 105 (2014) 166–176.
[44] Available at: https://baike.sogou.com/v4063060.htm?fromTitle=%E5%8D%8A%E8%83%B1%E6%B0%A8%E9%85%B8
[45] D. Cao, X.F. Jin, Z.M. Gong, L.L. Ma, Y.L. Liu, L. Zheng, Progress on selenium adsorption and tolerance mechanism of tea plant, Curr. Biotechnol., 7 (2017) 445–449.